JOURNAL OF PROPULSION AND POWER
Vol. 19, No. 1, January–February 2003

Combined/Simultaneous Gust and Oscillating Compressor Blade Unsteady Aerodynamics

Kuk Kim Frey* and Sanford Fleeter†
Purdue University, West Lafayette, Indiana 47907

Experiments are performed in a three-stage axial flow research compressor to investigate and quantify the simultaneous/combined gust- and motion-induced unsteady aerodynamic response of the first-stage rotor blades of the compressor. The gust-response unsteady aerodynamics are experimentally modeled with a 2 per revolution forcing function. The torsion mode unsteady aerodynamics is investigated utilizing an experimental influence coefficient technique in conjunction with a unique drive system. Combined gust and oscillating unsteady aerodynamics are obtained by the superposition of the oscillating blade row and the gust-response unsteady aerodynamics. Simultaneous gust- and motion-induced unsteady aerodynamic responses are obtained by driving the torsion mode oscillation in the presence of the 2 per revolution forcing function. The effects of steady loading are quantified. Airfoil oscillation amplitude effects are also studied. The combined unsteady aerodynamics establishes superposition limitations at high oscillation amplitudes and high loading. In addition, the gust–blade motion phase angle is identified as a key parameter.

Nomenclature

C_l^+	=	unsteady lift first harmonic
C_m^+	=	unsteady moment first harmonic
C_p^{n+}	=	first harmonic influence coefficient, nth rotor blade oscillating
$\hat{C}_p^+$	=	unsteady pressure first harmonic
$\hat{C}_p^+(x)$	=	unsteady pressure coefficient at location x
$\bar{P}$	=	rotor blade surface steady pressure
$\bar{P}_{ec}$	=	corrected static pressure at rotor midspan
p^+	=	first harmonic unsteady pressure, psi
u^+	=	first harmonic chordwise gust velocity
V	=	absolute flow velocity
v^+	=	first harmonic transverse gust velocity
		$\bar{y}$ half-height of the cam follower rise
v_{v+p}^+	=	measured transverse gust, vertical and potential components
$\bar{W}$	=	mean rotor inlet relative velocity
α'	=	time-variant rotor blade angular position
$\bar{\alpha}$	=	real-valued torsion oscillation magnitude or mean absolute flow angle
α^+	=	complex-valued torsion oscillation amplitude
ΔC_p	=	unsteady difference pressure first harmonic
ΔC_p^{n+}	=	first harmonic unsteady pressure
Δp	=	first harmonic unsteady differential pressure
Δp^{n+}	=	reference blade first harmonic unsteady pressure
ρ	=	mean air density
σ	=	interblade phase angle

Subscripts

p	=	potential
v	=	vertical

Superscripts

G	=	gust
M	=	oscillating blade motion
$+$	=	first harmonic

Introduction

FLOW-INDUCED vibrations, either forced response or flutter, cause blade high-cycle fatigue, with rotor blades particularly susceptible because of the large mean stresses from centrifugal forces. Flutter is a self-excited vibration, with the unsteady aerodynamics dependent on the blade motion. Forced vibrations are externally excited, with the forcing function that drives the blade motion independent of that motion.

In linearized models, the unsteady flow is considered to be a small perturbation to the mean flow. Furthermore, blade row unsteady aerodynamics are assumed to be harmonic, with each harmonic independent. Thus, the unsteady aerodynamic blade row response to a forcing function comprises two components: the gust response resulting from the disturbance being convected with the mean flow over nonresponding airfoils and the aerodynamic damping resulting from the airfoil response. With mechanical damping considerably reduced in advanced designs, the aerodynamic damping determines the response. Thus, it is important to investigate the motion-induced unsteady aerodynamics, the aerodynamic damping, for both flutter and forced vibrations.

Unsteady aerodynamic modeling is continually improving. However, the validity of the physical and mathematical assumptions, their limitations, and their range of applicability have yet to be established. New models are typically verified by correlating predictions with those of simpler models or with lightly loaded thin airfoil cascade data due to the lack of appropriate data. Also, the use of Navier–Stokes analyses in place of linearized analyses is accompanied by the need for significantly increased computational resources. Thus, the establishment of the applicability and the limitations of the various models is also necessary to determine the most efficient analysis for a particular application.

Experiments have been directed at either oscillating cascade or gust unsteady aerodynamics. However, there are significant differences in oscillating cascade aerodynamic damping experiments directed at flutter and forced response. For flutter, the issue is stability, with the aerodynamic damping determined over the complete range of interblade phase angles. For forced response, the key is vibration amplitude, with the aerodynamic damping required at a particular interblade phase angle.

Received 21 January 2002; revision received 11 September 2002; accepted for publication 11 September 2002.

*Rolls Royce Indianapolis, Lift Fan Gear Box Department, 2001 South Tibbs, T-24. Member AIAA.

†McAllister Distinguished Professor, School of Engineering, 1288 Mechanical Engineering; fleeter@ecn.purdue.edu. Fellow AIAA.

For experiments directed at gust model verification, if the assumptions inherent in the analyses are experimentally modeled, that is, thin low camber airfoils at near zero incidence with attached flow, then the data and predictions are generally in agreement. For low aspect ratio compressor blades operating at design, these models are appropriate. However, at actual operating conditions, that is, finite camber, steady loading, or nonzero incidence, the data-prediction correlations are not nearly as good.

Experiments have studied forcing functions,[1–3] with the key linear theory vortical gust characteristics identified.[4,5] When the experimental gust closely resembled a linear theory vortical gust, the correlation between the gust response data and predictions was excellent. However, most airfoil gusts do not resemble vortical gusts, and hence, there were poor correlation results. Another important finding was that the airfoil-generated static pressure field was of equivalent magnitude to the vortical gust. Thus, both the vortical and potential gust forcing functions must be considered.

Limited oscillating linear cascade data exist because of the difficulties associated with oscillating airfoils over a wide range of interblade phase angle values. This was overcome by developing an experimental influence coefficient technique.[6,7] Oscillating blade row unsteady aerodynamics was investigated in an isolated low-speed rotor, with the blades oscillated with constant amplitude at different interblade phase angles.[8] However, even though the amplitude of oscillation was small, the correlation of these data with linear theory[9] was poor as a result of leading-edge separation that was not modeled. The experimental influence technique has been successfully applied to a rotating blade row with attached flow, with both motion-dependent and gust-response data obtained.[7,10]

This paper presents, for the first time, the detailed experimental investigation of the combined and simultaneous motion- and gust-induced unsteady aerodynamic response of compressor rotor blades from both flutter and forced response perspectives. Specific objectives include the following: experimentally quantify the simultaneous and combined torsion motion and convected gust-generated unsteady aerodynamic response of compressor rotor blades and address the fundamental assumptions inherent in linear unsteady aerodynamic models, including the range of validity of the superposition principle and small perturbation models.

Experiments are performed in the extensively instrumented Purdue Axial Flow Research Compressor. Two plates in the inlet generate a periodic 2 per revolution gust forcing function to the first-stage rotor. The motion induced response is simulated by oscillating first-stage rotor blades in torsion with variable amplitudes of oscillation.

For oscillating blade experiments to be meaningful for forced response, the blade row must be oscillated at a specified interblade phase angle, and the oscillation and gust frequencies must match. The phasing problem and the high cost of oscillating airfoil experiments are overcome by an experimental influence coefficient technique.[6] The unsteady aerodynamics of an airfoil row oscillating at a constant interblade phase angle is obtained by oscillating only a single airfoil, with the airfoil response measured on the oscillating airfoil and its stationary neighbors. This is the unsteady aerodynamic influence coefficient $\Delta C_p^n(x)$. The unsteady aerodynamics of an equivalent blade row oscillating at all interblade phase angles σ are then determined mathematically:

$$\Delta C_p(x,\sigma) = \sum_{n=-N}^{N} \Delta C_p^n(x) e^{in\sigma} \tag{1}$$

The matching between the oscillation and gust frequencies is achieved with a unique cam follower mechanism design. Because both the gust generators and the cam that produces the rotor blade oscillatory motion are stationary, the gust excitation and blade oscillation frequencies are exactly matched and proportional to compressor speed.

Research Compressor

The Purdue Axial Flow Research Compressor models the fundamental turbomachinery unsteady aerodynamic phenomena, including the incidence angle, the velocity and pressure variations, the reduced frequency, and the rotor and stator row geometry and flow conditions. The compressor is driven by a 15-hp dc electric motor at a speed of 2000 rpm. Each identical stage contains 43 rotor blades and 31 stator vanes having a British C4 airfoil profile.

The rotor blade torsion mode drive system consists of three components: the blade assembly, the cam follower assembly, and the cam (Fig. 1). As the compressor rotates, the cam follower rides along the sinusoidal surface of a stationary cam, and its linear motion is translated into rotary motion via a lever arm fixed to the rotor blade. The elegance of this system is that the pitching motion of the rotor blades is achieved without employing any other motor drive systems: The mechanism oscillates the rotor blade as long as the compressor is operating. Also, the sinusoidal cam surface produces a single-frequency harmonic motion.

The angular deflection amplitude for these experiments is 10 deg or less. Hence, the blade torsion motion $\alpha'(t)$ is

$$\alpha'(t) \cong (\bar{y}/l)\sin\omega t = \bar{\alpha}\sin\omega t \tag{2}$$

The four rotor blades instrumented with dynamic pressure transducers, and blades $n = -2, -1, 0$, and 1 are individually oscillated (Fig. 2). This is accomplished with four identical mechanisms operated simultaneously. Individual blade oscillations are accomplished by indexing the endplate with the cam follower assemblies to the appropriate blades. Different height cams vary the torsion amplitude.

Instrumentation

The detailed instrumentation is shown in Fig. 2. The oscillating blade motion $\alpha'(t)$ is determined by a precision rotary potentiometer with voltage output linearly proportional to angular position. These data are accurate to within 0.15 deg. The first-stage rotor inlet flow is measured with a rotating cross hot wire mounted at blade midspan, 18.8% chord upstream of the blade leading edge and 65.5% span circumferentially from an adjacent rotor blade. The hot wire is calibrated for velocities ranging from 100 (30.5) to 200 ft/s (61.0 m/s)

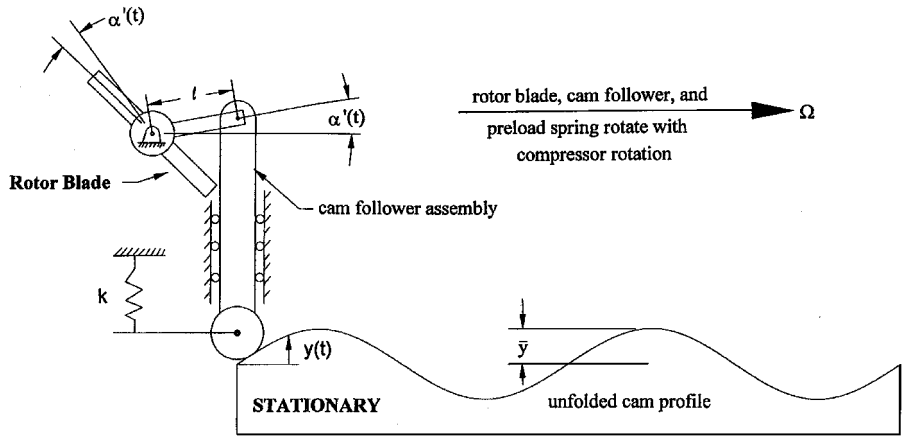

Fig. 1 Rotor blade oscillation mechanism.

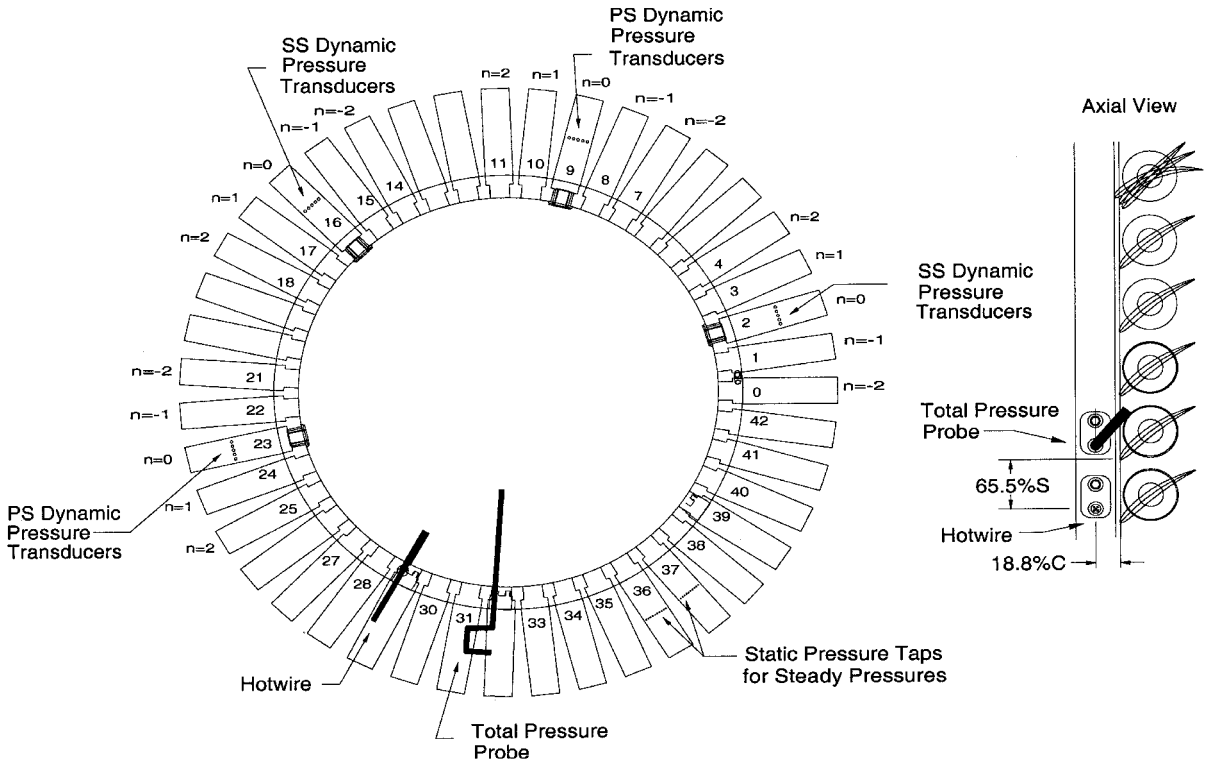

Fig. 2 Rotor instrumentation.

and flow angles ranging from −40 to +40 deg, with the velocity and flow angle uncertainty estimated to be 5% and ±0.5 deg.

The blade steady loading is obtained with a rotor-based Scanivalve system. Two blades are instrumented with 10 midspan static pressure taps, 1 pressure surface and 1 suction surface. The blade unsteady aerodynamics is obtained with 20 ultraminiature high-response pressure transducers installed at midspan on four blades. These transducers can operate to 10,000 *g* steady and 100 *g* of 2-kHz dynamic acceleration and are, thus, suitable for the experiment steady rotating (1018 *g*) and dynamic (50 *g* at 66.67 Hz) environments. The transducers are calibrated statically and dynamically, with a static calibration uncertainty of ±4%. Dynamic calibration for frequencies from 40 to 2700 Hz revealed a maximum gain and phase error of ±0.60 dB and ±1.5 deg.

Data Acquisition and Analysis

The rotor-based steady and unsteady data are transmitted to the stationary reference frame through a mercury-wetted slip ring. Low noise-to-signal ratio is achieved by amplifying the low amplitude dynamic pressure voltages 200 times.

The rotor blade instantaneous incidence is determined by superimposing the instantaneous incidence variation due to the blade oscillations on the measured gust incidence $i_{\text{gust}+\text{torsion}}(t) = i_{\text{gust}}(t) + i_{\text{torsion}}(t)$. The rotor blade oscillation mechanism is designed to provide a sinusoidal variation. However, the blades may not execute exactly harmonic motion due to manufacturing tolerances. Thus, a Fourier transform of $\alpha(t)$ is performed.

Blade Aerodynamic Response

The rotor blade loading is characterized by the steady pressure coefficient,

$$\bar{C}_p(x) = \frac{\bar{P}(x) - \bar{P}_{ec}}{\rho \bar{W}^2} \tag{3}$$

With the blade and reference pressures measured at different radii, a correction is applied to the exit static pressure to account for centrifugal effects. A correction is also applied to the rotor relative dynamic pressure because the velocity is measured in the rotor blade potential field.

The unsteady aerodynamic response to the gusts is characterized by the blade surface unsteady pressure coefficient,

$$\bar{C}_p^+(x) = \frac{p^+(x)}{\rho \bar{W}^2 v_{v+p}^+} \tag{4}$$

Blade surface unsteady pressures are Fourier decomposed, with the first harmonic pressure nondimensionalized by the unsteady dynamic pressure. Because the unsteady aerodynamic response is generated by both the vortical and potential gust components, the appropriate nondimensionalization parameter is the measured vortical-potential gust.

Blade Unsteady Pressures

The experimental influence coefficient technique is utilized, with only a single blade oscillated at a given time. Hence, the simultaneous gust and blade motion unsteady pressure data represent the gust response and the influence of the *n*th blade oscillating on the instrumented blade. The simultaneous data of interest are the all-blades-oscillating and the gust-induced unsteady aerodynamic response. Thus, the influence coefficient technique[6] is applied to the simultaneous gust and oscillating blade data:

$$p^{(G+M)^+} = \left\{ \sum_{n=-N}^{N} \left[p^{n(G+M)+} - p^{G+} \right] e^{in\sigma} \right\} + p^{G+} \tag{5}$$

If the gust-only unsteady pressure were not subtracted before the influence coefficient summation, then the combined response would have $2N$ times the gust response. Thus, the gust-only response is first subtracted from the simultaneous data, and then the influence coefficient summation is applied. The gust-only response is then added to determine the simultaneous gust and all-blades-oscillating aerodynamic response.

The combined gust and oscillating blade unsteady aerodynamic response is also determined by superposition. The dimensional gust-only generated unsteady pressure is added to the oscillating individual blade-only unsteady pressure,

$$p^{n(G+M)+} = p^{n(M)+} + p^{G+} \tag{6}$$

The superposition response for the combined gust and all blades oscillating is determined by first applying the influence coefficient technique to the oscillating blade influence pressures to determine the equivalent all-blades-oscillating response and then adding the gust-only response:

$$p^{(G+M)+} = p^{M+} + p^{G+} = \left\{ \sum_{n=-N}^{N} p^{n(M)+} e^{in\sigma} \right\} + p^{G+} \qquad (7)$$

The combined gust and oscillating blade unsteady pressure is nondimensionalized by the appropriate gust parameters: forced response, $\rho \bar{W}^2 (v^+/\bar{W})$; flutter, $\rho \bar{W}^2 \alpha^+$; and combined gust and blade motion, $\rho \bar{W}^2 \alpha^+ + \rho \bar{W}^2 (v^+/\bar{W})$. Note that the transverse gust velocity v is the measured quantity that consists of both the vortical and potential components. The unsteady differential pressure coefficient is determined by subtracting the suction surface from the pressure surface unsteady pressure coefficient, with the unsteady lift and moment coefficients then calculated.

Results

Experiments are performed directed at investigating and quantifying the simultaneous and combined gust- and motion-induced unsteady aerodynamic response, with the effects of steady loading and blade oscillation amplitude effects addressed.

Rotor Blade Steady Pressures

The first-stage rotor steady pressures with and without gust generators are presented in Fig. 3. The gust generators have no notable effect. The steady pressure distribution is a function of only loading. The surface pressures are predominantly affected by the front half-chord loading, with the pressure magnitude increased on the pressure surface and decreased on the suction surface. Increased loading results in increased pressure difference over the entire airfoil, particularly in the front half-chord.

Overall, the steady data agree well with SFLOW, a nonlinear potential code[11] and INCMCSCD, an incompressible inviscid small camber airfoil cascade analysis,[12] except near the leading edge. INCMCSCD predicts the maximum pressure difference location at low loading, but not at high loading. Adjustments were made to the rotor inlet flow angle for SFLOW to achieve good data matching: $\beta = 57.5$ deg and $M = 0.133$ for low loading and $\beta = 61.5$ deg and $M = 0.128$ for high loading. The high loading ΔC_p correlation with SFLOW is better than with INCMCSCD because SFLOW includes steady loading effects. Also note that INCMCSCD only predicts the pressure difference ΔC_p.

Instantaneous Rotor Blade Incidence

The blade torsion changes the gust-only instantaneous rotor incidence. The circumferential orientation of the various amplitude cams driving the blade motion is different relative to the fixed gust generators (Fig. 4). Hence, the effective combined gust–oscillating blade incidence is different for each oscillation amplitude.

$$i_{\text{gust}+\text{torsion}}(t) = i_{\text{gust}}(t) - \alpha(t) \qquad (8)$$

where the blade motion $\alpha(t)$ is distinguished from the oscillating blade incidence i_α by a 180-deg phase difference, that is, i_α is the negative of the oscillating blade position.

Figures 5–7 show the instantaneous incidence due to simultaneous gust and blade oscillations. The 3.5-deg blade oscillation incidence is nearly out-of-phase with the gust incidence (Fig. 5), thereby combining destructively to reduce incidence. The incidence due to the 90-deg gusts and the 5-deg-blade oscillation are neither in- nor out-of-phase. Rather, they combine constructively and destructively in various parts of the cycle (Fig. 6). The 10-deg-blade oscillation incidence is nearly in phase with the 90-deg-gust incidence (Fig. 7). Thus, the forcing functions combine constructively, resulting in larger incidence.

In terms of blade motion, the 3.5-deg-blade oscillations and 45-deg gusts generate gust–blade motion phase angles of 0.32 and −0.03 deg for low and high loading. The phase angle difference between the 45-deg gusts and the 5-deg-blade motion is −65 deg for low loading. For the 90-deg gusts and 10-deg-blade oscillation amplitude, the gust–blade motion phase angles are −140 and −130 deg for low and high loading. Because the instantaneous incidence directly affects the rotor aerodynamics, the phase angle between the gust and the blade motion is an important parameter in the combined gust and blade oscillation experiments.

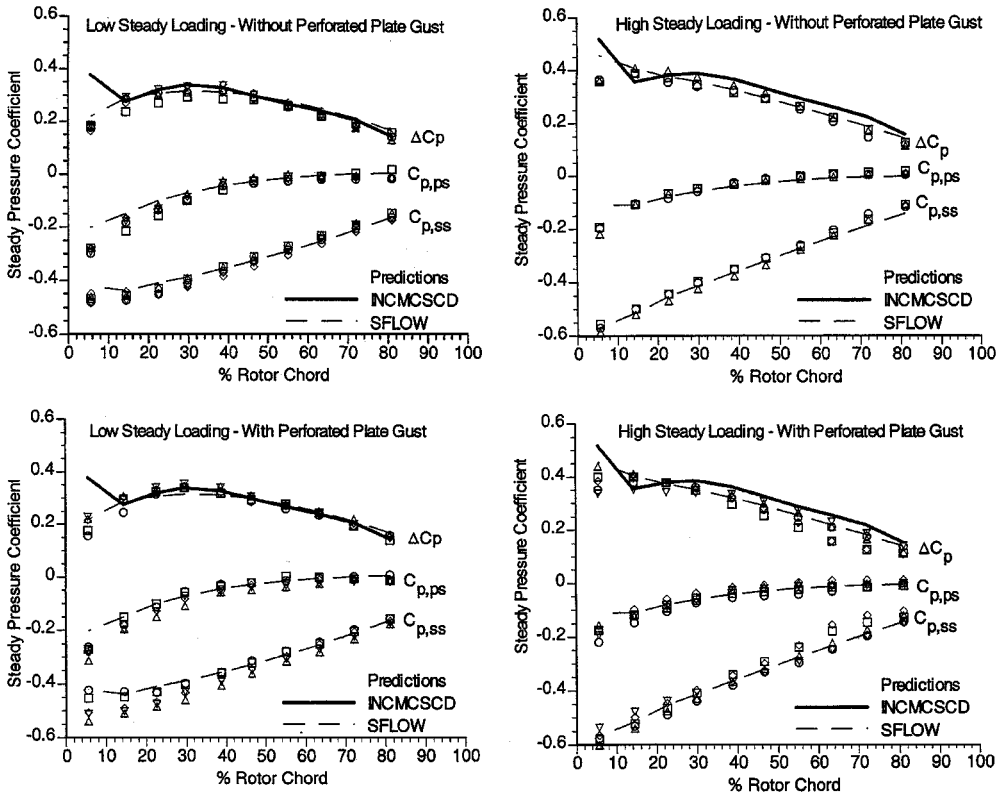

Fig. 3 Rotor blade surface steady pressures.

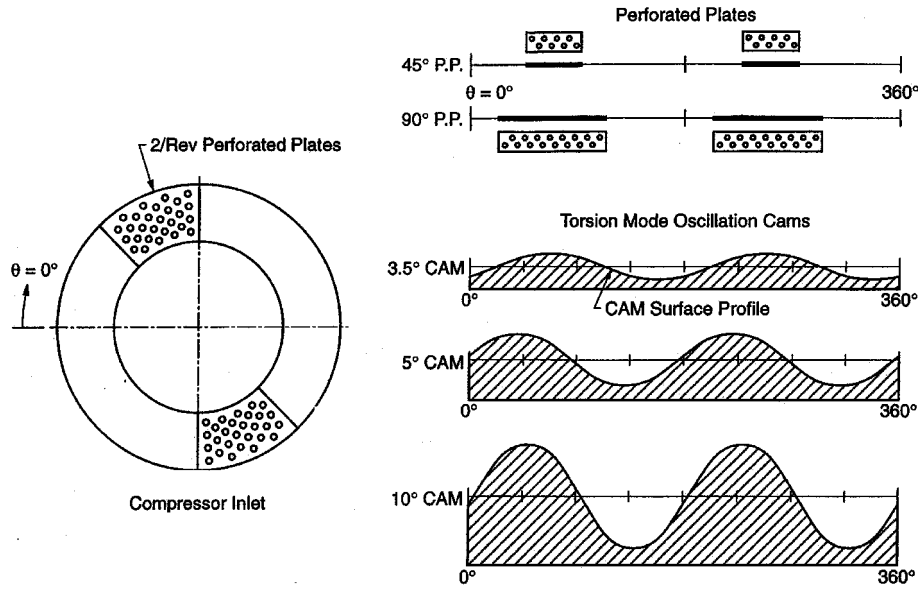

Fig. 4 Cam orientation with respect to plate gust generators.

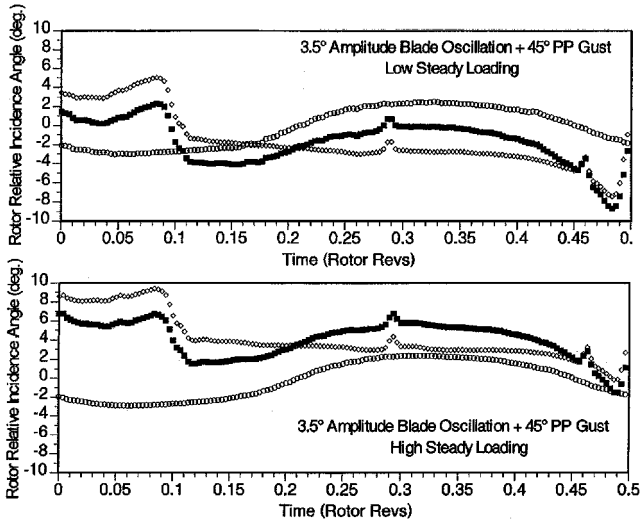

Fig. 5 Combined gust and 3.5-deg blade oscillation incidence i: ■, gust and oscillating blade; ○, oscillating blade; and ◇, gust.

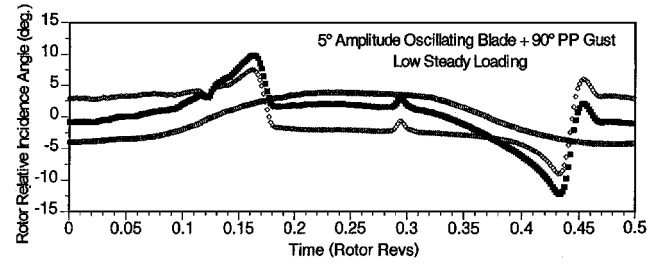

Fig. 6 Combined gust and 5-deg blade oscillation incidence i: ■, gust and oscillating blade; ○, oscillating blade; and ◇, gust.

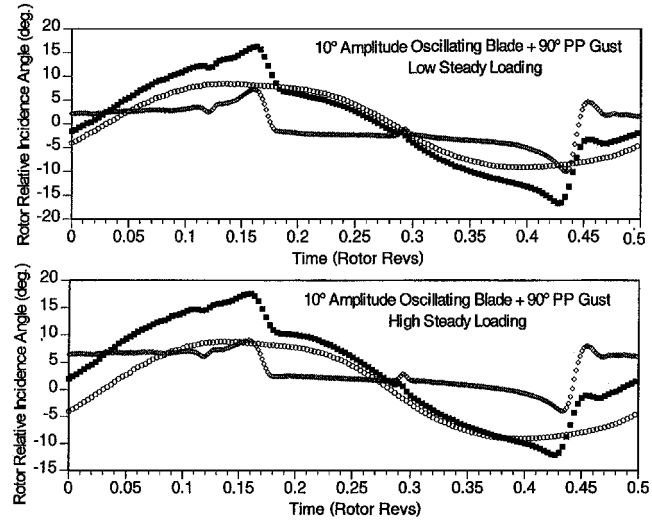

Fig. 7 Combined gust and 10-deg blade oscillation incidence i: ■, gust and oscillating blade; ○, oscillating blade; and ◇, gust.

Superposition Principle Assessment

The superposition principle is examined by comparing data obtained with simultaneous gust and oscillating blade excitations with the corresponding superposition data determined by summing the gust-only and oscillating-blade-only data. When the superposition principle is valid, the superposition data denoted by the filled symbols $[(G)+(T)]$ coincide with the simultaneous data denoted by the open symbols $[(G+T)]$ in Figs. 8 and 9. Note that the combined data are the sum of the gust-induced unsteady aerodynamics and the unsteady aerodynamic influence of the nth blade oscillating on the reference blade. The influence coefficient aerodynamics are used because they are the raw simultaneous data, allowing superposition to be investigated without influence coefficient summation errors. The simultaneous and superposition unsteady pressures are nondimensionalized by the combined gust and blade motion forcing function $\lfloor \rho \bar{W}^2 \alpha^+ + \rho \bar{W}^2 (v^+/\bar{W}) \rfloor$.

The validity of the superposition principle varies, primarily being a function of oscillation amplitude although also affected by loading (Figs. 8 and 9). Oscillation amplitude effects are revealed by the clustering of the unsteady lift and moment coefficient data for 3.5-deg-oscillation amplitude data (small symbols) and the spread of the corresponding 10-deg-oscillation amplitude data (large symbols). Higher loading results in only a small change in the unsteady lift and moment data, except for the 10-deg-blade oscillation data. For most oscillating blade positions, the agreement between the simultaneous and superposition data is poorer at the higher oscillation amplitude indicated by the greater differences in the largest size symbols.

The unsteady lift and moment coefficients obtained by superposition are normalized by the corresponding simultaneous data, denoted Ls/L and Ms/M in Fig. 10. They are generally within the data uncertainty for 3.5- and 5-deg-blade oscillation amplitudes at

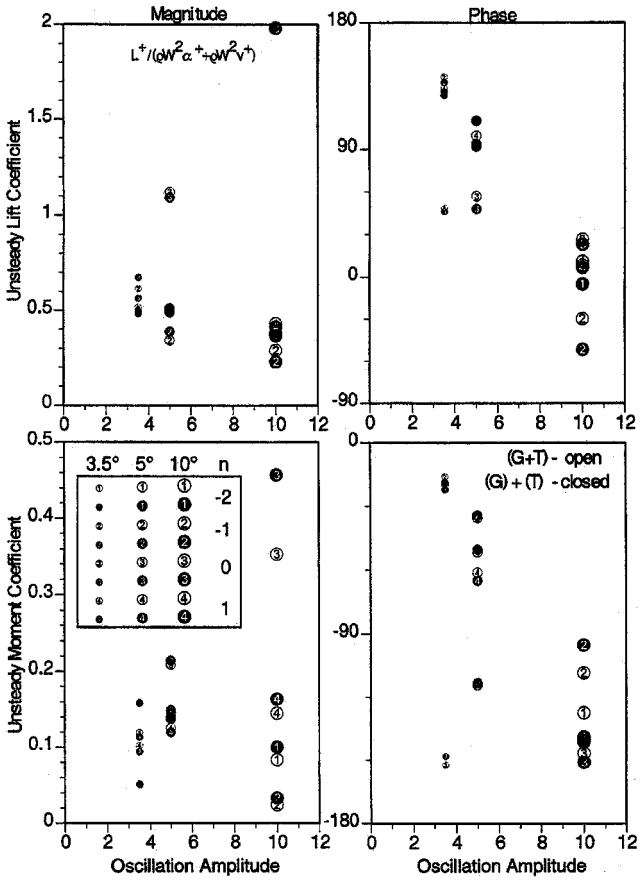

Fig. 8 Amplitude effect on combined gust and oscillating blade lift and moment at low loading.

low steady loading, with the correlation of the simultaneous and superposition unsteady moment data better than that for the unsteady lift. Superposition does fairly well at the 3.5-deg oscillation amplitude and high loading, with the exception of the $n = 0$ blade oscillating moment. Thus, even at the low amplitude of oscillation, the combination with the gust excitation produces a nonlinear response. However, with a 10-deg-oscillation amplitude, the simultaneous and superposition unsteady lift data correlate well but the unsteady moment data do not. Increasing the steady loading makes the simultaneous and superposition data correlation even poorer, in agreement with previous results.[7] Increasing the oscillation amplitude and steady loading also contribute to larger differences between the simultaneous and superposition data.

The applicability of the superposition principle is further assessed by correlating the simultaneous gust and all blades oscillating unsteady lift and moment data determined from the influence coefficient technique, with the corresponding superposition data, Table 1. Even after considering the uncertainty propagated by the influence coefficient summation, the superposition unsteady lift and moment coefficients do not correlate well with the simultaneous data at high steady loading. The superposition evaluation showed a stronger influence of oscillation amplitude than steady loading. However, in terms of gust and all-blades-oscillating unsteady aerodynamics, the applicability of superposition appears more sensitive to steady loading. This in fact may be an indication that the experimental influence coefficient is not valid at high steady loading, with high blade-oscillation amplitudes aggravating the matter.

Forced Response: Gust and Aerodynamic Damping

The combined gust and torsion unsteady aerodynamic data are analyzed to quantify the aerodynamic damping in terms of the unsteady aerodynamic lift and moment nondimensionalized by the unsteady gust parameter. The simultaneous/combined and the superposition/combined gust and oscillating blade aerodynamics are

Table 1 Combined gust and blade motion unsteady lift and moment coefficients

Superposition/data	C_l – superposition / C_l – simultaneous data	C_m – superposition / C_m – simultaneous data
3.5-deg torsion plus 45-deg perforated plate gust at low loading	$1.13\angle -6.3$ deg	$0.99\angle -108.5$
5-deg torsion plus 90-deg perforated plate gust at low loading	$1.09\angle -13.7$ deg	$1.13\angle -.50$ deg
10-deg torsion plus 45-deg perforated plate gust at low loading	$0.87\angle -11.01$ deg	$1.27\angle -3.35$ deg
3.5-deg torsion plus 45-deg perforated plate gust at high loading	$1.47\angle 5.79$ deg	$1.65\angle 99.97$ deg
10-deg torsion plus 90-deg perforated plate gust at high loading	$0.61\angle -1.88$ deg	$1.31\angle -6.26$ deg

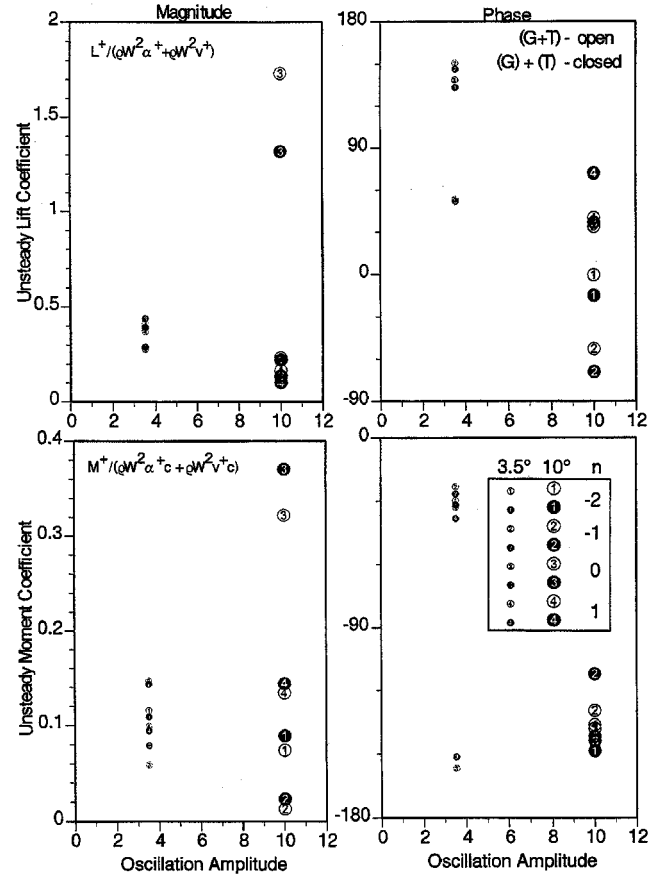

Fig. 9 Amplitude effect on combined gust and oscillating blade lift and moment at high loading.

considered, with the unsteady lift and moment coefficients determined from the following pressure definitions:

$$p^{(G+M)+} = \begin{cases} \left\{ \sum_{n=-N}^{N} \left(p^{n(G+M)+} - p^{G+} \right) e^{in\sigma} \right\} + p^{G+} & \text{simultaneous} \\ p^{M+} + p^{G+} = \left\{ \sum_{n=-N}^{N} p^{n(M)+} e^{in\sigma} \right\} + p^{G+} & \text{superposition} \end{cases} \tag{9}$$

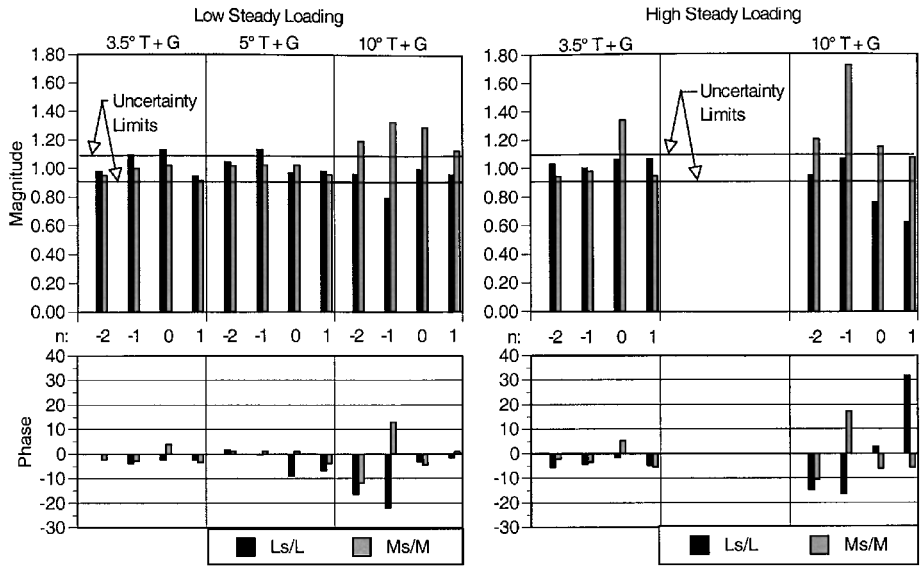

Fig. 10 Superposition/simultaneous combined gust and oscillating blade unsteady aerodynamics.

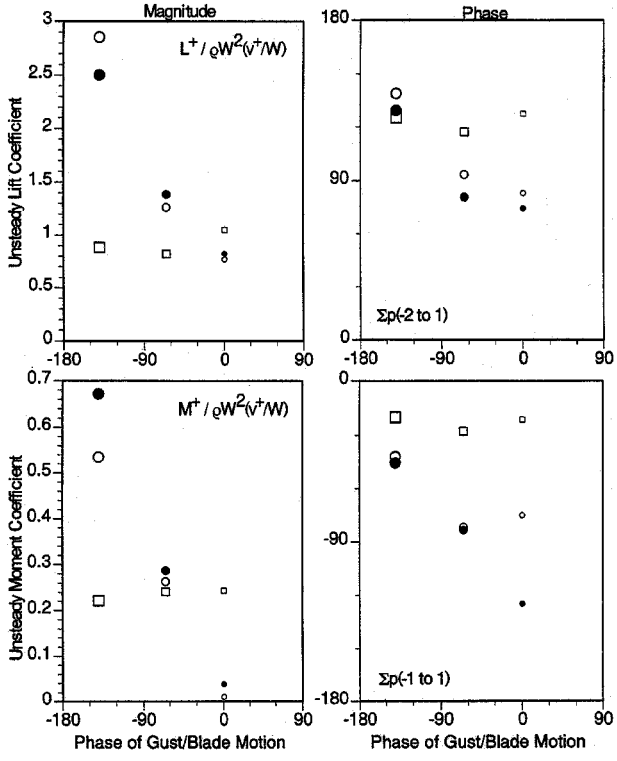

Fig. 11 Gust and oscillating blade motion phase effect on unsteady aerodynamics at low loading: oscillation amplitude, gust only: □, 3.5 deg; □, 5 deg; and □, 10 deg; $G+T=\Sigma[(G+T)-(G)]+G$: ○, 3.5 deg; ○, 5 deg; and ○, 10 deg; and $G+T=\Sigma T+G$: ●, 3.5 deg; ●, 5 deg; and ●, 10 deg.

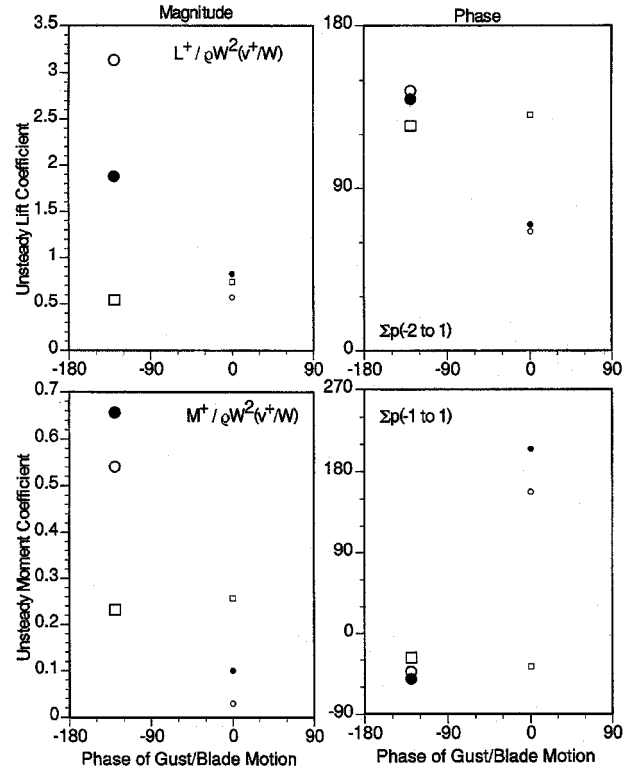

Fig. 12 Gust and oscillating blade motion phase effect on unsteady aerodynamics at high loading: oscillation amplitude, gust only: □, 3.5 deg; and □, 10 deg; $G+T=\Sigma[(G+T)-(G)]+G$: ○, 3.5 deg; and ○, 10 deg; and $G+T=\Sigma T+G$: ●, 3.5 deg; and ●, 10 deg.

The phase between the gust and the blade motion ($\phi_{v+}-\phi_\alpha$) was shown to be an important parameter. It is dependent on the blade structural characteristics and the forcing function frequency ratio Ω/ω_α and is, thus, fixed for a particular machine and flow conditions. However, the blade motion is mechanically imposed in these experiments. Hence, ($\phi_{v+}-\phi_\alpha$) is fixed for a given oscillation amplitude. The gust–blade motion phase angles are 0.32 and −0.03 deg for 3.5-deg-blade oscillations with low and high loading, −65 deg (295 deg) for 5-deg-blade oscillation at low loading, and −140 deg (220 deg) and −130 deg (230 deg) for 10-deg-blade oscillation with low and high loading.

Figures 11 and 12 show the effect of the gust–blade motion phase on the combined gust and oscillating blade unsteady lift and moment at low and high loading. Presented are the simultaneous and superposition data for comparison with the gust-only data. At low loading, combining the 3.5-deg amplitude oscillation with the 45-deg gust data, ($\phi_{v+}-\phi_\alpha$) = 0.32 deg, results in a 27% decrease in the unsteady lift magnitude and a phase shift of approximately −45 deg as compared to the gust-only data. When the 5- and 10-deg amplitude oscillations interact with the 90-deg gust, the unsteady lift magnitude increases significantly as compared to the gust-only data, on the order of two for the 5- and three for the 10-deg-oscillation amplitudes. However, the phase shift is smaller than the gust-only data. The high loading unsteady lift results are similar. Combining the high loading 3.5-deg amplitude oscillation with the 45-deg gust, ($\phi_{v+}-\phi_\alpha$) = −0.03 deg, the unsteady lift coefficient magnitude

decreases by 20% as compared to the gust-only data but shifts in phase by almost −60 deg. For the 10-deg amplitude oscillation and the 90-deg gust data, $(\phi_{v+} - \phi_\alpha) = -130$ deg, the combined lift magnitude increases by a factor of six and the phase increases by 20 deg.

The unsteady moment also changes significantly from the gust-only value, with the magnitude change dependent on the oscillation amplitude or the gust-blade motion phase. Combining the 3.5-deg amplitude oscillation with the 45-deg gust at low loading, the unsteady moment magnitude decreases by more than 80% to near zero, with the phase decreasing approximately −60 deg (Fig. 12). Combining the 5-deg amplitude oscillation and the 90-deg gust low loading data, $(\phi_{v+} - \phi_\alpha) = -65$ deg, the unsteady moment coefficient magnitude is only minimally affected, but the phase decreases by −60 deg. Combining the 10-deg amplitude oscillation and the 90-deg gust low loading data, $(\phi_{v+} - \phi_\alpha) = -140$ deg, the gust-only unsteady moment coefficient magnitude increases by a factor of two, but the phase decreases by only −30 deg. When Figs. 11 and 12 are compared, steady loading has a negligible effect on the combined gust and blade motion unsteady aerodynamics. The high steady loading results for the unsteady moment are similar.

Thus, a gust–blade motion phase near 0 deg results in an unsteady lift and moment decrease and a large phase shift as compared to the gust-only data. A gust–blade motion phase near −180 deg results in a large unsteady lift and moment increase but a small phase change. Hence, the gust–blade motion phase has a significant effect on the combined gust and aerodynamic damping unsteady aerodynamics.

The nonapplicability of superposition for the combined gust and blade motion unsteady aerodynamics is apparent in Figs. 11 and 12, indicated by the large differences between the superposition and the simultaneous data, particularly at the high-oscillation amplitudes. For the 3.5-deg oscillations and the 45-deg gust, the superposition and simultaneous unsteady lift magnitudes are in agreement at low loading but not at high loading. However, the superposition moment magnitude data do not agree well with the simultaneous data at either low or high loading. The superposition and simultaneous unsteady lift phase shifts at 3.5-deg-blade oscillation, particularly at high loading. However, in this particular case, it may not be superposition but rather that this phase difference is largely due to the combined gust and blade motion data having a small magnitude, making the phase measurement more difficult. With a 5-deg-oscillation amplitude, superposition works well for both the unsteady lift and moment. With a 10-deg-oscillation amplitude, superposition underpredicts the unsteady lift at low and high steady loading by 14 and 41%. However, the superposition unsteady lift phase agrees well with the simultaneous data. The superposition method overpredicts the moment at low and high steady loading by 26 and 22%. Thus, superposition is not applicable to high-oscillation amplitudes and high steady loading.

Because the gust–blade motion phase is different for each oscillation amplitude, there is some ambiguity as to whether the gust–blade motion phase or the oscillation amplitude itself is responsible for the differences in the combined gust and blade motion unsteady aerodynamics. The combined gust and blade motion forcing function data reveal that these differences are most likely due to the gust–blade motion phase. When the gust–blade motion phase is near 0 deg, the gust is in-phase with the blade motion but out-of-phase with the oscillating blade incidence. Thus, the gust unsteady aerodynamics destructively combines with the oscillating blade aerodynamics, a direct result of the gust interaction with the blade motion generated unsteady flow. At every instant, the rotor incidence changes with blade motion and with the gust. Thus, the instantaneous incidence to the rotor blade is different than that for the gust forcing function only.

For a 3.5-deg-oscillation amplitude, the gust–blade motion phase is such that the incidence change due to the blade motion cancels or decreases the blade incidence due to the gust-only, Fig. 5. Therefore, decreased unsteady lift and moment magnitudes result. With a 5-deg-oscillation amplitude, the incidence resulting from the blade motion is such that it both increases and decreases the instantaneous incidence due to the gust at different points of the blade oscillation (Fig. 6). The resulting instantaneous incidence is increased overall as compared to that due to the gust-only, but not as much as if the gust–blade motion interaction was completely constructive. Thus, the unsteady lift and moment magnitudes increase marginally due to the blade motion interacting with the gust. For the 10-deg-oscillation amplitude, the gust–torsion phase is such that almost a complete constructive interaction occurs (Fig. 7). Thus, the unsteady lift and moment magnitudes increase significantly with very little change in phase.

Table 2 Gust–blade motion phase angle effect on interacting gust and blade motion unsteady lift

	Unsteady lift	
Interacting gust and blade motion	Magnitude range	Phase range, deg
3.5-deg torsion plus 45-deg perforated plate gust at low loading	0.2 to 2.0	110
5-deg torsion plus 90-deg perforated plate gust at low loading	0.0 to 1.7	300
10-deg torsion plus 45-deg perforated plate gust at low loading	0.7 to 2.5	360
3.5-deg torsion plus 45-deg perforated plate gust at high loading	0.1 to 1.6	360
10-deg torsion plus 90-deg perforated plate gust at high loading	0.8 to 1.9	360

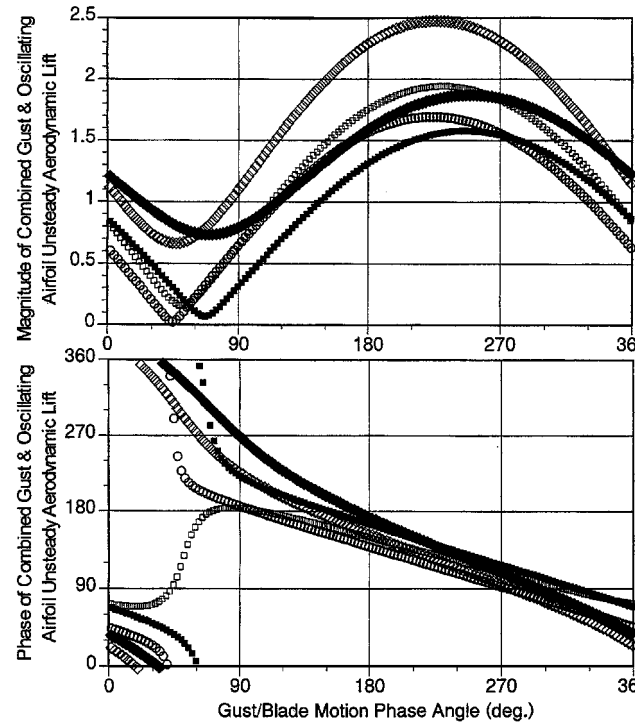

Fig. 13 Gust–blade motion phase effect on combined gust and oscillating blade lift: □, 3.5-deg oscillating airfoil and 45-deg perforated plate gust at low loading; ○, 5-deg oscillating airfoil and 90-deg perforated plate gust at low loading; ◇, 10-deg oscillating airfoil and 90-deg perforated plate gust at low loading; ■, 3.5-deg oscillating airfoil and 45-deg perforated plate gust at high loading; and ◆, 10-deg oscillating airfoil and 90-deg perforated plate gust at high loading.

The unsteady aerodynamics due to the combined gust and oscillating blade are strongly influenced by the gust–blade motion phase. Figure 13 shows the variation in the unsteady lift as a function of the gust–blade motion phase angle with these results also summarized in Table 2. In general, the unsteady lift range of values varies, dependent on the relative magnitudes of the aerodynamic damping and the gust unsteady aerodynamics.

These interacting gust and oscillating blade unsteady aerodynamic results suggest the possibility of controlling the gust–blade motion phase to reduce the blade row unsteady aerodynamic loading. Furthermore, these data indicate that superposition may not be

applicable for forced response when the vibration amplitudes are large and at high steady loading, particularly for gust–blade motion phase angles such that the gust and aerodynamic damping combine constructively.

Flutter: Gust and Aerodynamic Damping

The effect on stability of combining the gust and oscillating blade aerodynamics is considered, with stability specified by the sign of the unsteady aerodynamic work. When it is positive, the flowfield supplies energy to the blade row, and hence, the blade row is unstable. For an oscillating blade row, a gust changes the unsteady aerodynamics, thereby potentially affecting its stability.

To investigate gust–oscillating blade interactions on stability, the gust and blade motion data interblade phase angles and frequencies must match. Also, the combined gust and blade motion unsteady lift and moment are nondimensionalized by the oscillating blade parameter, $\rho \bar{W}^2 \alpha^+$, with the unsteady lift and moment coefficients determined per the pressure definitions of Eq. (9). Note that the blade row is stable when the phase of the unsteady aerodynamic moment is between 0 and 180 deg.

Figures 14 and 15 show the combined gust and oscillating blade unsteady lift and moment coefficients as a function of the gust–blade motion phase together with the oscillating blade-only data. At low steady loading, the blade motion unsteady lift magnitude is decreased by nearly 20%, whereas the phase is increased by almost 90 deg when the 45-deg gusts interact with the 3.5-deg oscillating blade. With a 5-deg-oscillation amplitude at low steady loading, a −65-deg gust–blade motion phase results in a 45% increase in the blade motion-only lift magnitude and a 50-deg phase shift. With a 10-deg-oscillation amplitude at low steady loading, a −140-deg gust–blade motion phase nearly doubles the blade motion-only unsteady lift magnitude and shifts the phase by 10 deg. As compared to the blade motion-only data, the gusts decrease the unsteady moment magnitude to near zero for the 3.5-deg-blade oscillations but increases 10 and 15% for the 5- and 10-deg-oscillation amplitudes.

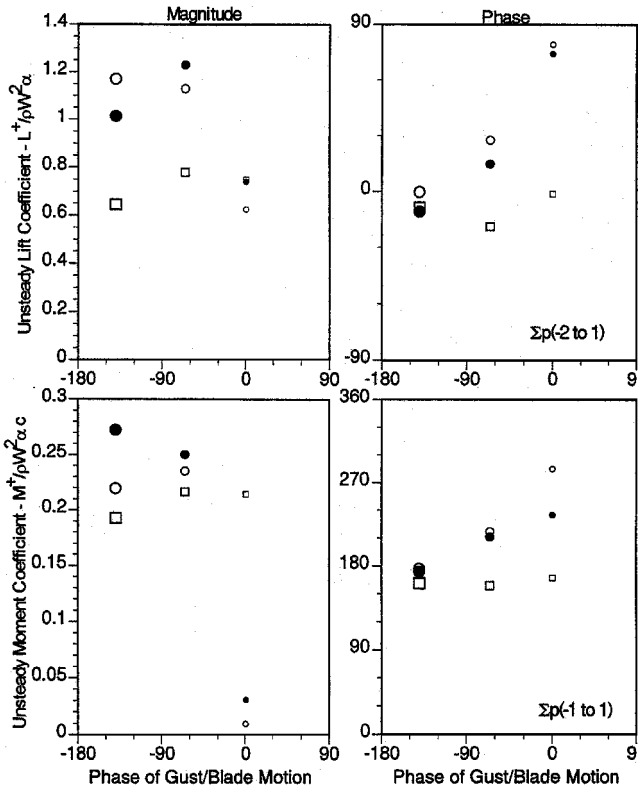

Fig. 14 Gust and oscillating blade phase effect on aerodynamic damping at low loading: oscillation amplitude, oscillating airfoils only: □, 3.5 deg; □, 5 deg; and □, 10 deg; $G+T=\Sigma[(G+T)-(G)]+G$: ○, 3.5 deg; ○, 5 deg; and ○, 10 deg; $G+T=\Sigma T+G$: ●, 3.5 deg; ●, 5 deg; and ●, 10 deg.

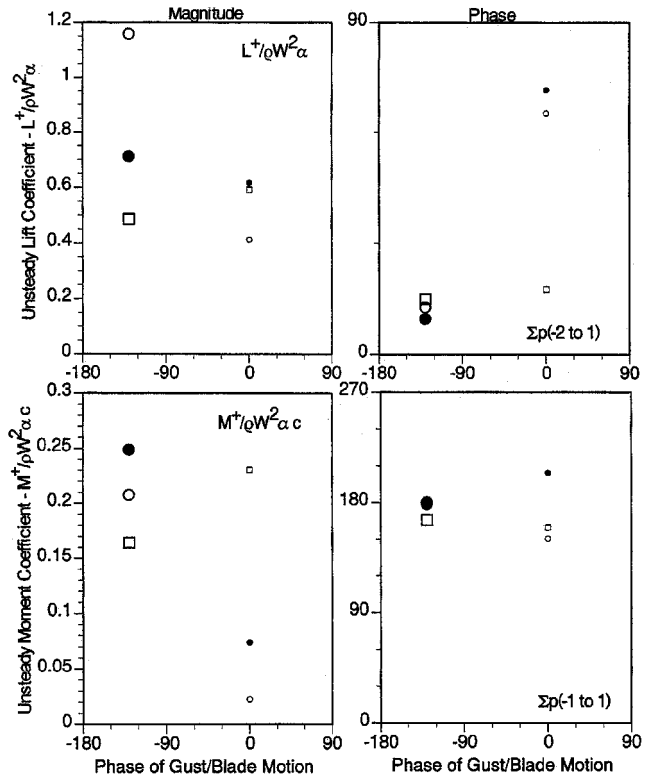

Fig. 15 Gust and oscillating blade phase effect on aerodynamic damping at high loading: oscillation amplitude, oscillating airfoils only: □, 3.5 deg; and □, 10 deg; $G+T=\Sigma[(G+T)-(G)]+G$: ○, 3.5 deg; and ○, 10 deg; $G+T=\Sigma T+G$: ●, 3.5 deg; and ●, 10 deg.

With increasing oscillation amplitude, the all blades oscillating unsteady lift and moment coefficients are essentially unaffected by the gust, with the small differences due to the nonlinear large-oscillation amplitude effects discussed earlier. The oscillating blade-only unsteady aerodynamic moment phase is approximately 170 deg, corresponding to stability but near the 180-deg boundary. When gust interacts with the oscillating blade, the resulting combined unsteady moment phase is increased by 120, 60, and 15 deg for the 3.5-, 5-, and 10-deg-blade oscillation amplitudes, respectively, with these combined gust and blade motion unsteady aerodynamics corresponding to instability.

The high steady loading results are similar. At 10-deg-oscillation amplitude, a −130-deg gust–blade motion phase results in a 15-deg increase of the oscillating airfoil-only unsteady moment phase, thereby corresponding to instability. In contrast to the low loading 3.5-deg-oscillation amplitude 45-deg gust results, the high loading moment phase is between 0 and 180 deg, corresponding to increased stability over that of the oscillating blade only.

Thus, stability is affected by the gust, with this effect dependent on the gust–blade motion phase. When the gust-blade motion phase is near 0 deg, the blade row becomes unstable at low loading but remains stable at high loading. As the gust–blade motion phase approaches −180 deg, there is a smaller shift in the combined unsteady moment phase. However, even this shift may destabilize a nominally stable blade row.

Figures 14 and 15 also show that superposition can lead to errors in evaluating the effect of the gust interacting with the oscillating blade, evident by the differences between the superposition data (dark symbols) and the simultaneous data (light symbols). In particular, consider the 3.5-deg amplitude oscillation high loading results. The superposition data predict instability, with the simultaneous data showing the opposite.

Figure 16 shows that the gust–blade motion phase should be between 20 and 180 deg for stability. These gust and blade motion unsteady aerodynamic effects are a direct result of the rotor incidence change caused by the interacting unsteady aerodynamic forcing functions. Similar to the forced response aerodynamic damping

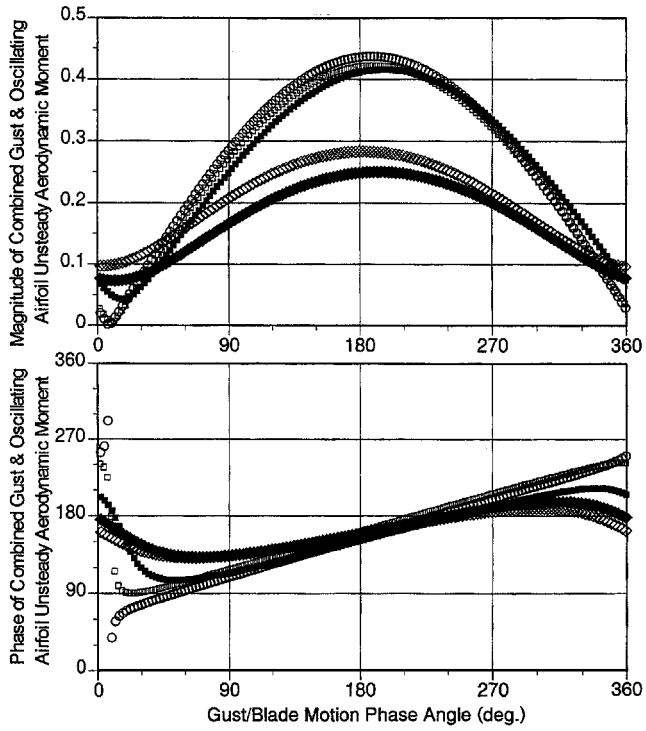

Fig. 16 Gust–blade motion phase effect on combined gust and oscillating blade moment: □, 3.5-deg oscillating airfoil and 45-deg perforated plate gust at low loading; ○, 5-deg oscillating airfoil and 90-deg perforated plate gust at low loading; ◇, 10-deg oscillating airfoil and 90-deg perforated plate gust at low loading; ■, 3.5-deg oscillating airfoil and 45-deg perforated plate gust at high loading; and ◆, 10-deg oscillating airfoil and 90-deg perforated plate gust at high loading.

and gust unsteady aerodynamics, a gust–blade motion phase that results in a constructive unsteady aerodynamic interaction leads to increased unsteady lift and moment magnitudes, whereas a destructive interaction leads to decreased magnitudes. The unsteady lift and moment phase angles are controlled by leading or lagging the gust excitation with respect to the blade motion. The gust–blade motion phase angle could be controlled by appropriately indexing the gust generators with respect to the blade motion.

Summary

Experiments were performed in the Purdue 3-Stage Axial Flow Research Compressor to investigate and quantify the simultaneous/combined gust- and motion-induced unsteady aerodynamic response of compressor first-stage rotor blades for both forced response and flutter. The gust unsteady aerodynamics were experimentally modeled with a 2 per revolution forcing function to the first-stage rotor blade row, generated by two perforated plates installed in the compressor inlet. The torsion mode unsteady aerodynamics were investigated utilizing an experimental influence coefficient technique in conjunction with a unique drive system that provides rotor blade torsion mode oscillations without other motor drive systems. The combined gust and oscillating unsteady aerodynamics were determined by the superposition of the separate oscillating blade row and gust response unsteady aerodynamics. The simultaneous gust- and motion-induced unsteady aerodynamic response were obtained by driving the torsion mode oscillation in the presence of the 2 per revolution forcing function.

The combined gust and oscillating blade unsteady aerodynamic response established the applicability limits of superposition at high-oscillation amplitudes and high loading, with superposition generally leading to underprediction of the unsteady lift but an overprediction of the unsteady moment. Also, the combined gust and oscillating blade unsteady aerodynamics were significantly influenced by the gust–blade motion phase angle. Gust–blade motion phase angles resulting in a constructive interaction of the gust with the oscillating blade aerodynamics increased the unsteady lift and moment magnitudes with small changes in phase. In contrast, a gust–blade motion phase angle resulting in a destructive interaction decreased the unsteady lift and moment magnitudes with large changes in phase. Thus, these results show that neglecting aerodynamic damping can lead to serious errors in forced response prediction, depending on the gust–blade motion phase angle. Also, combining a gust excitation with an oscillating blade row could alter the blade row stability, depending on the gust–blade motion phase angle.

Acknowledgments

This research sponsored, in part, by the Army Research Office. This support is most gratefully acknowledged. The truly exceptional design and manufacturing support from Ronnie D. McGuire is also gratefully appreciated and acknowledged.

References

[1]Manwaring, S. R., and Fleeter, S., "Forcing Function Effects on Rotor Periodic Aerodynamic Response," *ASME Journal of Turbomachinary*, American Society of Mechanical Engineers, Vol. 113, No. 2, 1991, pp. 312–319.

[2]Kim, K. H., and Fleeter, S., "Compressor Blade Row Unsteady Aerodynamic Response to Attached and Separated Flow Forcing Functions," *International Journal of Turbo and Jet Engines*, Vol. 11, Nos. 2–3, 1994, pp. 201–218.

[3]Kim, K. H., and Fleeter, S., "Forcing Function Generator Fluid Dynamic Effects on Compressor Blade Gust Response," *Journal of Propulsion and Power*, Vol. 10, No. 2, 1994, pp. 204–216.

[4]Henderson, G. H., and Fleeter, S., "Forcing Function Effects on Unsteady Aerodynamic Gust Response, Part 1: Forcing Function," *ASME Journal of Turbomachinary*, American Society of Mechanical Engineers, Vol. 115, No. 4, 1993, pp. 741–750.

[5]Henderson, G. H., and Fleeter, S., "Forcing Function Effects on Unsteady Aerodynamic Gust Response, Part 2: Low Solidity Airfoil Row Response," *ASME Journal of Turbomachinary*, American Society of Mechanical Engineers, Vol. 115, No. 4, 1993, pp. 751–761.

[6]Buffum, D. H., and Fleeter, S., "Oscillating Cascade Aerodynamics by an Experimental Influence Coefficient Technique," *Journal of Propulsion*, Vol. 6, No. 5, 1990, pp. 612–620.

[7]Frey, K. K., and Fleeter, S., "Oscillating Airfoil Aerodynamics of a Rotating Compressor Blade Row," *Journal of Propulsion and Power*, Vol. 17, No. 2, 2001, pp. 232–239.

[8]Hardin, L. W., Carta, F. O., and Verdon, J. M., "Unsteady Aerodynamic Measurements on a Rotating Compressor Blade Row at Low Mach Number," American Society of Mechanical Engineers, ASME Paper 87-GT-221, June 1987.

[9]Verdon, J. M., and Caspar, J. R., "Subsonic Flow Past an Oscillating Cascade with Finite Mean Flow Deflection," *AIAA Journal*, Vol. 18, No. 5, 1980, pp. 540–548.

[10]Frey, K. K., and Fleeter, S., "Rotating Compressor Blade Row Gust Unsteady Aerodynamics," AIAA Paper 98-3435, July 1998.

[11]Hoyniak, D., and Verdon, J. M., "Development of a Steady Potential Solver for Use with Linearized Unsteady Aerodynamic Analyses," *Unsteady Aerodynamics, Aeroacoustics, and Aeroelasticity of Turbomachines and Propellers*, edited by H. M. Atassi, Springer-Verlag, New York, 1991, pp. 177–194.

[12]Henderson, G. H., and Fleeter, S., "Oscillating Aerodynamics and Flutter of an Aerodynamically Detuned Cascade in an Incompressible Flow," *International Journal of Turbo and Jet Engines*, Vol. 10, No. 4, 1993.